



Analysis of acute brain slices by electron microscopy: A correlative light–electron microscopy workflow based on Tokuyasu cryo-sectioning



Celine Loussert Fonta^{a,*}, Andrew Leis^b, Cliff Mathisen^c, David S. Bouvier^{d,1}, Willy Blanchard^a, Andrea Volterra^d, Ben Lich^c, Bruno M. Humbel^a

^a Electron Microscopy Facility, University of Lausanne, Biophore, 1015 Lausanne, Switzerland

^b CSIRO, Australian Animal Health Laboratory, Private Bag 24, Geelong 3220, Australia

^c FEI Company, Achtseweg Noord 5, 5651 GG Eindhoven, The Netherlands

^d Department of Fundamental Neurosciences, University of Lausanne, Rue du Bugnon 9, 1005 Lausanne, Switzerland

ARTICLE INFO

Article history:

Received 18 July 2014

Received in revised form 16 October 2014

Accepted 20 October 2014

Available online 8 November 2014

Keywords:

Correlative light–electron microscopy

Acute brain slice

Tissue

Tokuyasu cryo-sectioning

Immunolabelling

Astrocyte

Green fluorescent protein (GFP)

Scanning transmission electron microscopy

(STEM)

ABSTRACT

Acute brain slices are slices of brain tissue that are kept vital *in vitro* for further recordings and analyses. This tool is of major importance in neurobiology and allows the study of brain cells such as microglia, astrocytes, neurons and their inter/intracellular communications via ion channels or transporters. In combination with light/fluorescence microscopies, acute brain slices enable the *ex vivo* analysis of specific cells or groups of cells inside the slice, e.g. astrocytes. To bridge *ex vivo* knowledge of a cell with its ultrastructure, we developed a correlative microscopy approach for acute brain slices. The workflow begins with sampling of the tissue and precise trimming of a region of interest, which contains GFP-tagged astrocytes that can be visualised by fluorescence microscopy of ultrathin sections. The astrocytes and their surroundings are then analysed by high resolution scanning transmission electron microscopy (STEM). An important aspect of this workflow is the modification of a commercial cryo-ultramicrotome to observe the fluorescent GFP signal during the trimming process. It ensured that sections contained at least one GFP astrocyte. After cryo-sectioning, a map of the GFP-expressing astrocytes is established and transferred to correlation software installed on a focused ion beam scanning electron microscope equipped with a STEM detector. Next, the areas displaying fluorescence are selected for high resolution STEM imaging. An overview area (e.g. a whole mesh of the grid) is imaged with an automated tiling and stitching process. In the final stitched image, the local organisation of the brain tissue can be surveyed or areas of interest can be magnified to observe fine details, e.g. vesicles or gold labels on specific proteins. The robustness of this workflow is contingent on the quality of sample preparation, based on Tokuyasu's protocol. This method results in a reasonable compromise between preservation of morphology and maintenance of antigenicity. Finally, an important feature of this approach is that the fluorescence of the GFP signal is preserved throughout the entire preparation process until the last step before electron microscopy.

© 2014 The Authors. Published by Elsevier Inc. This is an open access article under the CC BY license (<http://creativecommons.org/licenses/by/3.0/>).

1. Introduction

Despite the increased use of *in vivo* recordings on conscious animals to provide new insights into cellular neurophysiology, acute brain slices remain the tool of choice for patch clamp recording

to analyse biological features such as ion channels and calcium flux (Khurana and Li, 2013). Since their introduction 50 years ago by Henry McIlwain (Collingridge, 1995; McIlwain, 1958), acute brain slices have been studied in detail by using advanced fluorescence microscopy techniques such as Stimulated Emission-Depletion (STED) microscopy, Stochastic Optical Reconstruction Microscopy (STORM) and Photoactivated Localization Microscopy (PALM), bringing the resolution under the micrometre level (Huang et al., 2010). Even more recently, a combination of two photon excitation and pulsed STED microscopy (Bethge et al., 2013) improved the imaging resolution on acute brain slices to a point-spread function

* Corresponding author.

E-mail address: Celine.Loussert@unil.ch (C. Loussert Fonta).

¹ Present address: Centre for Research in Neuroscience, Department of Neurology and Neurosurgery, The Research Institute of the McGill University Health Centre, Montreal General Hospital, QG H3G 1A4, Canada.

of 62 nm for 40 nm fluorescent beads. However, one disadvantage of these imaging techniques is that only fluorescent structures (labelled or auto-fluorescent) can be observed and the reference structure needs to be fluorescently counterstained (Griffiths, 2001; Schwarz and Humbel, 2007). For this reason, electron microscopy is still the preferred method to observe subcellular organisation of biological samples. This is also due to its higher resolving power and when used in conjunction with gold immunolabelling, specific proteins can be localised and studied within their context, as the subcellular structure is directly visible (Schwarz and Humbel, 2007).

Electron microscopy analysis of acute slices (Kirov et al., 1999; Takano et al., 2014) combined with the low magnification overview and localisation capabilities of light/fluorescence microscopy, i.e. correlative light–electron microscopy, appears the most appropriate way to access the complexity of biological samples (Loussert et al., 2012; Mironov and Beznoussenko, 2009; Modla and Czymmek, 2011; Robinson and Takizawa, 2009). The light micrograph can supply *in vitro* analysis or maps of the regions of interest displaying for instance a fluorescent signal, which can then be imaged at higher resolution in an electron microscope. Nevertheless, correlating light and electron micrographs has proven to be challenging due to the different constraints imposed by the type of microscopy performed. To ensure easy transfer of a precisely located biological region from the light microscope to the electron microscope, we developed a complete process based on the cryo-sectioning method for sample preparation established by Tokuyasu (Griffiths et al., 1983; Slot and Geuze, 2007; Tokuyasu, 1973). This method was chosen for two main reasons:

- (1) The type of fixation is suitable for immunolocalisation;
- (2) The absence of dehydration and resin embedding preserves GFP fluorescence throughout the entire process.

The aim of the protocol was to identify and recover the cells of interest during all processing steps from the original location in the organ to nanometre-scale observation in the electron microscope. As a model system, we chose mouse brain from transgenic animals, which expressed eGFP in astrocytes (Nolte et al., 2001). The first step of our protocol involved slicing the brain into thick vibratome sections. From that point onwards, the GFP-expressing astrocytes could be observed at all steps during sample preparation, ultrathin cryo-sectioning until high-resolution imaging by electron microscopy.

2. Materials and methods

2.1. Animal experiments

All animal work was carried out according to the recommendations of the Swiss Federal Laws on animal experimentation, approved by the Cantonal Veterinary Office (Vaud, Switzerland). All efforts were made to minimise suffering.

2.2. Tissue preparation

Adult wild type mice and adult eGFP-GFAP mice (Nolte et al., 2001) were anaesthetised with isoflurane in a closed chamber and euthanased by decapitation. The brain was removed and placed in ice-cold, gassed (95% O₂, 5% CO₂) Artificial CerebroSpinal Fluid (ACSF) medium containing 118 mM NaCl, 2 mM KCl, 1.3 mM MgCl₂, 2.5 mM NaHCO₃, 1.2 mM NaH₂PO₄ and 10 mM glucose, pH 7.4. Thick coronal sections of 300 µm containing hippocampus were then cut with a vibratome (Leica VT1200, Leica Microsystems, Vienna, Austria) and immediately transferred into phosphate buffer (0.1 M pH 7.4) containing 4% formaldehyde and 0.5% glutaral-

dehyde. Fixation was done for 2 h at room temperature, then the samples were stored in fixative for 12 h at 4 °C. The slices were washed in 0.1 M sodium phosphate buffer (PB: pH 7.4) and cut into small pieces. Each piece of sample was isolated and cryo-protected by infiltration with 2.3 M sucrose in 0.1 M sodium phosphate buffer (PB: pH 7.4) overnight at 4 °C.

2.3. Imaging

Brain slices in fixative solution were imaged with a Zeiss Imager.Z2 fluorescence microscope (Carl Zeiss Microimaging GmbH, Germany) equipped with an AxioCam MRC5 digital CCD camera (Carl Zeiss). Bright-field images and fluorescence images using filter set 38, excitation BP 470/40, beam splitter FT 495, emission BP 520/50 (Carl Zeiss) were acquired sequentially at the same focal plane through the entire volume. The brain slice was imaged with a 100 µm step in Z (through the entire depth of the tissue) with 2.5× objective (Carl Zeiss Microimaging Inc.; Plan-Neofluar, NA = 0.075) using the MosaiX module of the Zeiss Axiovision rel.4.8 software (Carl Zeiss).

Sucrose infiltrated brain pieces, mounted on aluminium pins, were imaged with the same Zeiss Imager.Z2 fluorescence microscope with 10× objective (Carl Zeiss; Plan-Neofluar, NA = 0.3) with 5 µm steps in Z and 20× objective (Carl Zeiss; Plan-Neofluar, NA = 0.5) with 1 µm steps in Z. During acquisition, the samples were kept hydrated and ice cooled to avoid dehydration. This was achieved by mounting the pins in a hole drilled into a Petri dish filled with ice. After imaging, the samples were immediately plunged into liquid nitrogen and stored until further processing.

2.4. Cryo-sectioning and fluorescence imaging of the thawed sections

For cryo-sectioning, pins with frozen brain tissue were mounted in a modified cryo-ultramicrotome (Ultracut UC6/FC6, Leica Microsystems, Vienna, Austria). The original binocular was replaced by a M205 FA stereo-fluorescence microscope equipped with a DFC 345 FX camera (Leica, Heerbrugg, Switzerland), suspended on a large swing arm (Leica, Heerbrugg, Switzerland). Tissue blocks were trimmed at –90 °C with a cryotrim diamond knife (Diatome, Biel, Switzerland) and ultrathin cryo-sections, 70 and 100 nm thick, were cut at –110 °C with an immuno diamond knife (Diatome). Sections were picked up with a drop containing an equal mixture of 2% methylcellulose and 2.3 M sucrose (Liou et al., 1996), warmed up to room temperature, and transferred onto a Formvar film-coated, carbon-stabilised 100 mesh copper finder grid (Electron Microscopy Sciences, Hatfield, PA, USA).

100 nm thin cryo-sections collected on grids were incubated four times for 2 min on a PBS solution to remove the methylcellulose/sucrose mix and then mounted on a glass microscope slide in PBS. This slide was overlaid with a glass coverslip and the cryo-sections were examined immediately with the Zeiss Imager.Z2 fluorescence microscope in bright-field mode and with GFP filters using 20× air (Carl Zeiss, Plan-Neofluar, NA = 0.5) and 40× oil objectives (Carl Zeiss, Plan-Neofluar, NA = 1.3).

Alternatively, sections were imaged with an epifluorescence microscope (CorrSight, FEI Company Eindhoven, The Netherlands) equipped with a ORCA-03G camera (Hamamatsu, Hamamatsu City, Japan) in bright-field mode and with GFP filter set using 5× air (Carl Zeiss, EC Plan-Neofluar, NA = 0.15), 20× air (Carl Zeiss, EC Plan-Neofluar, NA = 0.5) and 40× air (Carl Zeiss, EC Plan-Neofluar, NA = 0.9) objectives. Imaging was driven by a correlative and automated acquisition software ('Maps', FEI Company Eindhoven, The Netherlands).

2.5. GFP immuno-gold labelling

The temporary slide preparations were disassembled and immunogold labelling was performed to detect the GFP. First, the grids were washed 5 times in PBS for 2 min each, then incubated 5 min in PBS buffer containing 1% BSA (Aurion, Wageningen, The Netherlands) as a blocking step. Sections were floated for 1 h on a drop of primary antibody, chicken anti-GFP at 100 µg/ml (Abcam ab13970, Cambridge, UK) in PBS containing 1% BSA. After washing with 0.1% BSA in PBS, the samples were incubated for 1 h with 15 nm colloidal gold-conjugated secondary antibodies, goat anti-chicken (Aurion) diluted 1:30 in 1% BSA/PBS. The ultra-thin cryo-sections were then fixed in 1% glutaraldehyde in PBS for 10 min to further stabilise them, followed by eight washes in distilled water, 2 min each. Finally, the cryo-sections were embedded in a thin film of methylcellulose containing 0.3% uranyl acetate and air-dried.

2.6. VGLUT1 immuno-gold labelling

Immunogold labelling was performed to detect the VGLUT1 protein on ultrathin sections (70 nm thickness) or semi thin sections (100 nm thickness). Cryosections were picked up, warmed to room temperature, and transferred onto copper 'finder' grids (Electron Microscopy Sciences, Hatfield, PA, USA) as described above. Immunolabelling was performed using polyclonal guinea pig anti-VGLUT1 (synaptic systems, Goettingen, Germany) dilution 1/100 and with 10 nm colloidal gold-conjugated secondary antibodies, goat anti-guinea pig, (Aurion, Wageningen, The Netherlands) diluted 1:30 as described above.

2.7. STEM imaging

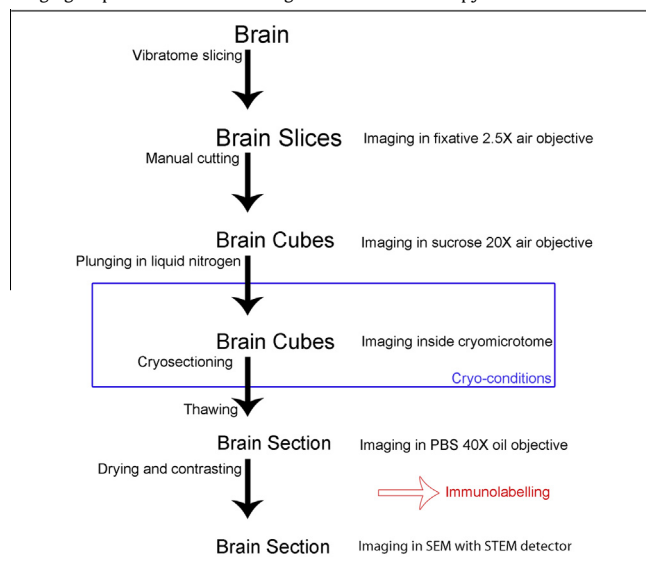
EM grids were mounted on a STEM sample holder and inserted into a Helios Nanolab 650 DualBeam (electron and ion) microscope (FEI Company, Eindhoven, The Netherlands). Imaging was driven by the same correlative and automated acquisition software ('Maps', FEI Company) as used with the CorrSight microscope and samples were imaged at 5 mm working distance. Overviews of the grids were taken in secondary electron mode at 30 keV with an Everhart–Thornley detector. Micrographs were then correlated with the images recorded with the 40× oil-immersion or air objectives in the light microscope. Areas containing regions of interest (ROIs) were pre-irradiated with an electron beam of 30 keV at current densities of 13 nA or 26 nA using a scan speed of 50 ns per pixel and a scan area of 4096 × 3536 pixels for 30 min per field of view. For imaging, we used a STEM III detector (FEI Company) in bright-field or high-angle annular dark-field mode with corresponding parameters of 30 keV, 400–800 pA, 1–3 µs dwell time and 6144 × 4096 pixels per frame. In the bright field mode, the contrast conditions are the same as for the bright field TEM. Where HAADF micrographs were recorded, the contrast was inverted to ease the observation and the correlation with bright field images. The large area, e.g. 66 µm × 57 µm, images were recorded with the Maps software (1.0; FEI Company) and stitched either with the Maps software or using Photoshop CS5 (Adobe). The Maps software stitches could be saved as HD View (Microsoft; <http://research.microsoft.com/en-us/um/redmond/groups/ivm/hdview/>) images and the Photoshop stitched images were saved as TIFF files.

2.8. TEM tomography

100 nm thick cryo-sections were imaged with a Tecnai-12 transmission electron microscope (FEI Company) operating at 120 kV. A dedicated dual-axis tomography holder (E.A. Fischione Instruments, Inc., Corporate Circle Export, USA) was used. Series

Table 1

Summary of the sample processing. The diagram describes the sample processing and imaging steps for the correlative light–electron microscopy workflow.



of single tilted images from -65° to $+65^\circ$ were acquired with a tilt increment of 1° using SerialEM software (Mastrorarde, 2005) (Boulder Laboratory, Boulder, USA) on a 4 K × 4 K Eagle CCD camera (FEI Company). Tomograms and surface representations were processed with the tomography software IMOD (Kremer et al., 1996) (Boulder Laboratory, Boulder, USA).

A summary of the entire workflow is presented in Table 1 with all the imaging steps.

3. Results and discussion

The robustness of this correlative light electron microscopy workflow is based on the possibility to image the sample using fluorescence excitation, and then track the area of interest at each processing step prior to electron microscopy. A large range of devices is available to image the fluorescence at room temperature but the imaging during the cryo-trimming and the cryo-sectioning was not possible. Conventional cryo-microtomes are equipped with a binocular that does not allow fluorescence imaging. We removed the optical part, replaced it with a fluorescence stereomicroscope (Fig. 1A) and installed the microtome in a dark room. We chose a system combining large depth of field and good resolution. This technical feature is important for the spatial rendering and it is indispensable for the cryosectioning. The position of the sample relative to the edge of the knife must be known for trimming and sectioning. We selected a Plan Achromat objective of 0.8×, NA 0.14 with a working distance of 112 mm to ease the manipulation inside the cryo-chamber (removal of debris, cryo-ribbon handling and cryosection collection) (Fig. 1B). This configuration is also important to keep the optical components outside of the cryo-chamber and to prevent any damage from repeated cooling and warming cycles. To optimise the sample visibility, we inclined the microscope at an angle of approximately 20° from the vertical (Fig. 1C). A swing arm stand with vibration-damping foot was used to stabilise the microscope during operation of the microtome (Fig. 1C). To limit the ice contamination during sectioning, the set up was installed in an enclosed room with a system controlling the humidity (Fig. 1D).

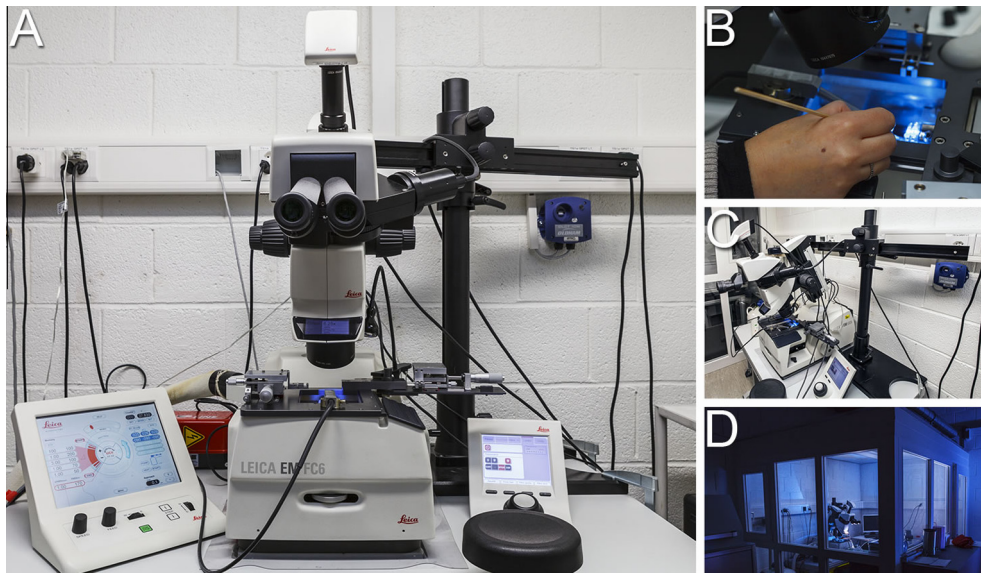


Fig. 1. Setup of the fluorescence cryo-microtome. (A) To observe the fluorescent area of interest during sectioning, the standard binocular system is replaced by a higher resolution fluorescence stereo-microscope. (B) The use of a long working distance objective (112 mm) allows sufficient clearance for manipulations inside the cryo-chamber. (C) The microscope is hanging on a swing arm stand with a vibration-damping foot. (D) To control sectioning conditions and allow fluorescence observations, the microtome is installed in a temperature and humidity controlled cabinet in a dark room.

This “homemade” setup can be easily reproduced in laboratories performing cryo-sectioning, and it proved to be a key element for various correlative approaches.

The preparation method developed by Kiyoteru Tokuyasu (Tokuyasu, 1973, 1976, 1978) was chosen to analyse the acute slices. This method, combining mild chemical fixation with cryo-sectioning, was continuously improved over the years to become the most commonly used technique for immuno-electron microscopy (Slot and Geuze, 2007). To prevent the risk of hypoxia and tissue damage (Kirov et al., 1999) during fixation, due to a slow diffusion rate of glutaraldehyde, we used a mixture of formaldehyde and glutaraldehyde. Under these conditions the small formaldehyde molecules rapidly penetrate and temporarily fix the specimen until the slower penetrating glutaraldehyde irreversibly crosslinks the proteins (Hayat, 1981).

Brain tissues fixed by perfusion were previously analysed by the Tokuyasu technique (Stephan et al., 2008, 2013) but this is the first time that acute slices, fixed by immersion, are analysed by this technique. Immediately after cutting, the slices were plunged into the fixative solution then processed further. The influence of the perfusion fixation versus the immersion fixation on the ultrastructure of hippocampal brain slices was investigated recently by electron microscopy (Takano et al., 2014), and the authors confirmed good preservation of the brain slice that were plunged immediately into fixative solution after slicing.

Various electron micrographs of acute brain slice prepared according to the Tokuyasu cryosectioning method are shown in Fig. 2. In panel 2A, we observe three synapses (arrows). Careful inspection of the micrograph confirms good preservation of the ultrastructure of the sample without any obvious extraction artefacts. Note that the cryo-sectioning method is particularly suitable for visualising membranes, vesicles (asterisks, Fig. 2A) and mitochondria (arrowheads, Fig. 2A).

The advantage of this approach is that antigens are more readily immunolabelled in cryosections than in resin sections (Stierhof et al., 1986). To confirm the preservation of antigenicity, we performed Vesicular Glutamate Transporter 1 (VGLUT1) immunolocalisation (Fig. 2B, C and D). As shown previously, the VGLUT1 protein was localised in asymmetric synapses, characterised by

the presence of a presynaptic and a postsynaptic element. The presynaptic axonal bouton, enriched in synaptic vesicles (arrowheads) could easily be identified on the micrograph (Fig. 2B) as well as the synaptic cleft (asterisk). The postsynaptic densities were also clearly identified (arrows).

To gain insight into the 3D distribution of vesicles inside the synapse, tilt series of a 100 nm section were acquired (Fig. 2C and Movie S1) (Zeuschner et al., 2006), then reconstructed (Fig. 2D and Movie S2) and modelled (Fig. 2E). The vesicles (Fig. 2E, yellow) were easily seen in the sections of the tomogram (Fig. 2D, Movie S2) and their distribution inside the presynaptic axonal bouton could be estimated. A multivesicular body (Fig. 2E, white) and mitochondrion (Fig. 2E, blue) were also reconstructed on the tomogram.

Although there are a number of publications showing the retention of GFP fluorescence in methacrylate resin embedded samples (Kukulski et al., 2011, 2012; Luby-Phelps et al., 2003; Nixon et al., 2009; Slot and Geuze, 2007), the advantage of cryosectioning is that proteins remain hydrated at physiological pH during sample processing thereby guaranteeing the preservation of fluorescence intensity (Slot and Geuze, 2007; Tsien, 1998). To investigate the preservation of the fluorescence in samples prepared according to the Tokuyasu method, we studied acute brain slices of a transgenic animal expressing eGFP under the control of the GFAP promoter (Nolte et al., 2001).

The fixed brain slices were first imaged by epifluorescence microscopy to map the GFP expressing astrocytes in the tissue. The most prominent feature (Fig. 3A) was the inhomogeneous distribution of the GFP signal over the slice. We observed areas that displayed intense fluorescence and others with no signal at all. Nolte et al. (Nolte et al., 2001) previously reported this result and they reasoned that the promoter used for this construct is transiently expressed in all astrocytes. Therefore, we must take into account that GFP expression may be an imperfect representation of the total astrocyte distribution in the brain with the consequence that all GFP expressing cells are astrocytes but not all astrocytes express GFP.

Based on the fluorescence distribution over the entire brain slice, we defined 7 areas characterised by various fluorescence

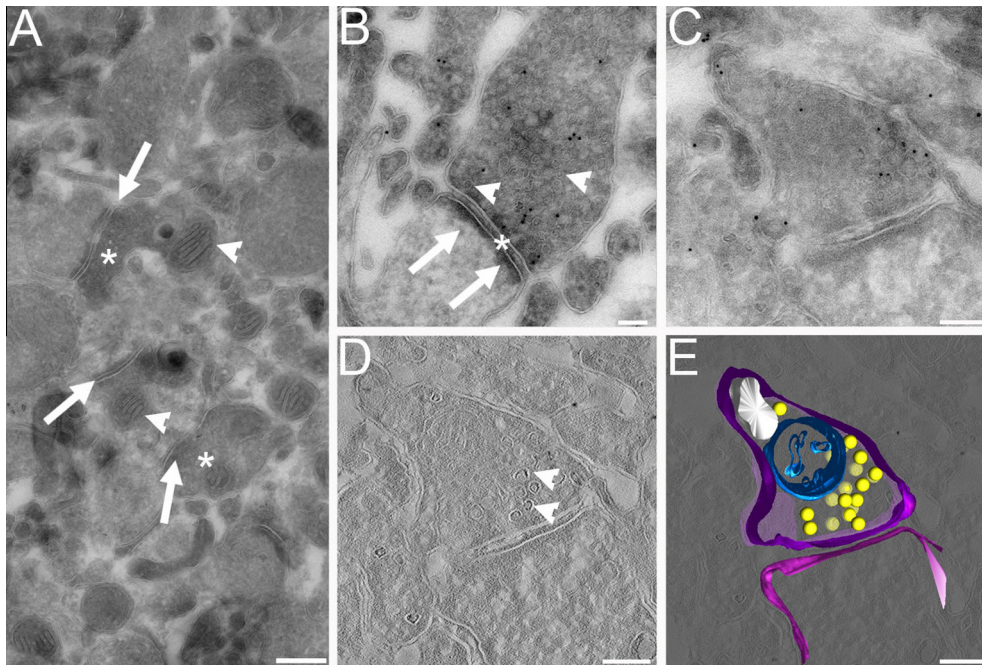


Fig. 2. Transmission electron micrographs of brain prepared according to the Tokuyasu cryo-sectioning method. (A) Overview of three asymmetric synapses (arrows) inside the brain tissue. All cells displayed a dense cytoplasm and numerous organelles like mitochondria (arrowheads), and vesicles (asterisks). The method of preparation based on the Tokuyasu method provided an excellent contrast of membranes, which is favourable to study intracellular vesicles. (B) Asymmetric synapse immunolocalised with anti-VGLUT1 antigen. The presynaptic axonal bouton, enriched with synaptic vesicles (arrowheads) is separated from the postsynaptic cell by the synaptic cleft (asterisks). The postsynaptic density is also clearly identified (arrows). (C) 0° tilt micrograph from tilt series of an asymmetric synapse immunolocalised with anti-VGLUT1 antigen (100 nm thick section) (see [Movie S1](#)). (D) Central section of the reconstructed tomogram obtained from the tilt series presented in C. The membranes of the vesicles are easily observed in the 3D volume (arrowheads) (see [Movie S2](#)). (E) Model of the asymmetric synapse presented in C displaying the distribution of the vesicles (yellow) inside the volume of the synapse. One multivesicular body (white) and a mitochondrion (blue) are also reconstructed. Scale bars represent: $A = 400$ nm, $B = 125$ nm, $C = 125$ nm, $D/E = 125$ nm.

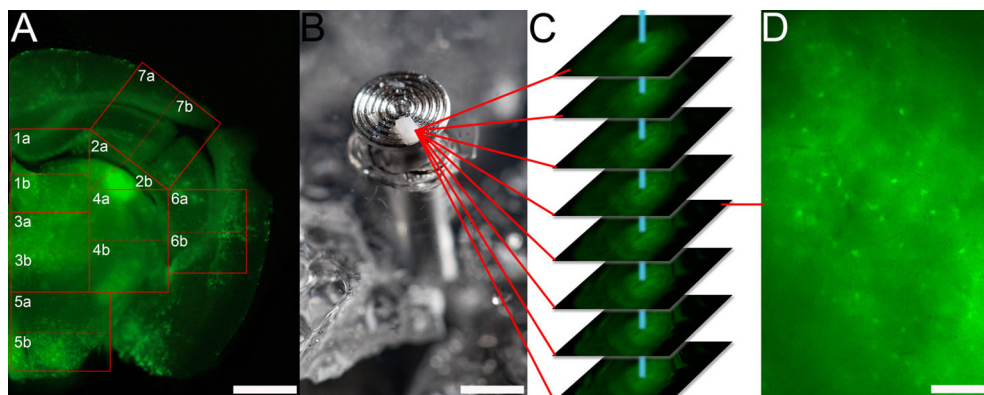


Fig. 3. Coronal slice of brain, 300 μm thick, containing GFP-expressing astrocytes and 3D mapping of the brain piece. (A) The chemically fixed brain slice (immersion fixation) was imaged by fluorescence microscopy to map the GFP-expressing astrocytes. Seven areas of interest were defined and divided into two parts, each measuring less than 1 mm^2 . For the analysis presented here, area 2b was selected. (B) A brain piece sitting on the aluminium pin, the holder for the cryo-ultramicrotome, is kept hydrated and cold during imaging using a plastic Petri dish containing ice cubes and a hole to hold the pin. (C) 3D stack of the brain piece recorded by wide-field fluorescence microscopy with an automated 3D acquisition system at a step size of 5 μm with a $10\times$ objective ([Movies S3 and S4](#)). (D) 60 μm below the block surface, many cell bodies were in focus. Scale bars represent: $A = 0.75$ mm, $B = 2$ mm and $D = 0.1$ mm.

patterns, each divided into 2 parts smaller than 1 mm^2 ([Fig. 3A](#)). Each piece of tissue was marked, cut out and then infiltrated in a sucrose solution. This step is essential in the Tokuyasu method for the preservation of the sample ultrastructure during freezing and cryo-microtomy. It requires a tissue piece smaller than 1 mm^3 to ensure optimal sucrose infiltration. The sucrose prevents the formation of visible ice crystals in the sample during freezing by reducing the amount of free water. Sucrose is also known to improve sectioning properties. In addition, it acts as a clearing

agent, making the tissue more transparent for light microscopy, enabling imaging to a depth of up to 300 μm (personal communication, Dr. Matthias Langhorst).

Each piece of tissue was mounted on an aluminium pin ([Fig. 3B](#)), used as a holder for microtomy and then imaged by epifluorescence microscopy in three dimensions (X, Y and Z; [Fig. 2C](#)) to precisely localise the GFP expressing astrocytes in the volume ([Fig. 2D](#)). Since tissue blocks shrink to an unpredictable degree during sucrose infiltration it was important to

image the fluorescence after sucrose infiltration to establish a reliable localisation of the GFP positive astrocytes in the 3D volume.

To avoid sample drying during imaging, we used a small device (an ice-filled plastic Petri dish with a hole drilled in the top) supporting the aluminium pin that kept the tissue cold and humid (Fig. 3B). Imaging was performed from top to bottom of the block using low magnification air objectives. We acquired image stacks of the entire volume of all pieces. The brain tissue of area 2b (Fig. 3A), located near the centre of the block, displayed numerous cell bodies expressing GFP (Fig. 3C, D and Movie S3), was selected as an example of the method developed herein. We determined that the majority of GFP-expressing astrocytes were at the depth of about 60 μm inside the sample and the X and Y position of the area of interest was defined. This provided the 3D coordinates of the GFP-astrocytes of interest inside the brain tissue. All tissue blocks were imaged in the same way (Movie S4). After imaging, the tissue sitting on the aluminium pin was plunged into liquid nitrogen and stored frozen at -80°C . Storage time of the sample is virtually unlimited under these conditions. If necessary the sample could be thawed, re-infiltrated with sucrose and then imaged again by fluorescence microscopy.

The pin with the frozen block was mounted on the sample holder inside the cryo-chamber of the cryo-ultramicrotome for trimming and ultra-thin sectioning. The cryo-microtome was modified (Fig. 1A) by replacing the original binocular with a higher resolution fluorescence stereo-microscope. In this way, the fluorescence signal of the astrocytes could be observed during all trimming and cutting steps. The key element of the cutting step was the 3D map of the brain piece. Astrocytes localised previously

in the volume of tissue pieces could then be reached using their X , Y and Z coordinates. The brain block imaged inside the cryo-chamber of the microtome (Fig. 4A) was first trimmed in the Z direction by removing 60 μm of tissue from the top to the previously identified area containing a large number of GFP-expressing cell bodies. During this trimming step, we used the fluorescence stereo-microscope to ensure that the area of interest was not removed. A frustum of pyramid with a face of $350\ \mu\text{m} \times 350\ \mu\text{m}$, containing the cells of interest was then trimmed. Numerous cell bodies on the surface of the tissue block could be visualised (Fig. 4B), confirming the quality of the 3D map established previously. Due to some inaccuracy in the Z position (about 1 μm), 100 nm thick serial cryo-sections were cut to ensure that the target was captured. The cryo-sections were picked up using an equal mixture of methylcellulose and sucrose. This mixture was selected because it limits stretching of the cryo-sections, thereby reducing extraction of cellular components (Liou et al., 1996). The grids were then stored in a cold and humid chamber before processing to avoid any drying artefacts. To image fluorescence of the sections, the grids were mounted between a glass slide and coverslip (Fig. 5A) as described previously (Takizawa and Robinson, 2003). A high numerical aperture (NA) oil-immersion objective (NA = 1.3) was used to acquire the 2D map of the sections. We observed a strong fluorescent signal corresponding to the cell bodies (Fig. 5B, arrowheads) and the thin processes of the GFP-expressing astrocytes. Cryosections of other areas displayed a more discrete fluorescent signal, in accordance with the inhomogeneous distribution of GFP astrocytes in the brain slice (Movie S4 and Fig. 2). The 100 nm thickness of the section is much thinner than the depth of focus of the high-NA objectives (0.5–1 μm) (Schwarz and Humbel, 2007), therefore no

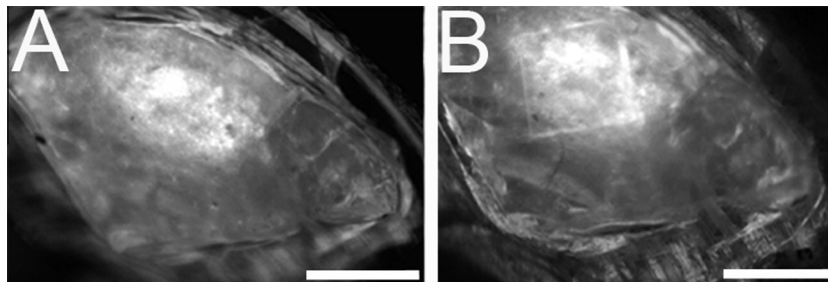


Fig. 4. Fluorescence imaging during cryo-sectioning. The piece 2b of the brain was imaged with the stereomicroscope before (A) and after trimming of the frustum of the pyramid (B). Scale bars represent: A/B = 350 μm .

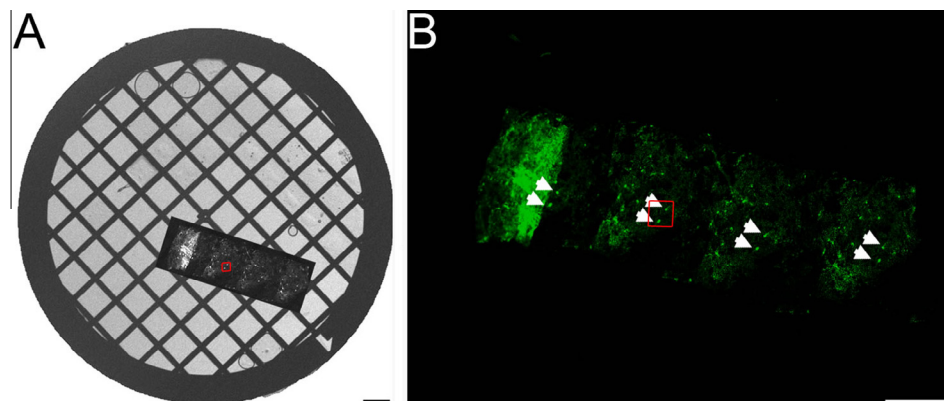


Fig. 5. 2D mapping of GFP astrocytes on the section. (A) Using a light microscope, an entire electron microscopy grid was imaged at low magnification (2.5 \times in bright-field mode). Then, a mosaic of the fluorescent section was recorded (20 \times). The manual overlay of the two images is presented here. (B) A higher resolution fluorescence mosaic was recorded with a 40 \times , 1.3NA oil objective. This image provided a map for electron microscopy investigation. Note the four, consecutive sections. Arrowheads indicate the cells of interest. The red squares in A and B indicate the area imaged at high resolution and presented in Fig. 7. Scale bars represent: A = 230 μm , B = 150 μm .

out-of-focus background fluorescence could be observed and fine details of the sample could be recorded. It is noteworthy that the fluorescence of the GFP appeared to be unaffected by the sample preparation. In the case of a classical preparation (strong chemical fixation, dehydration, resin embedding) it is more difficult to preserve GFP fluorescence.

The fluorescence imaging was done sequentially. First, an overview of the EM grid was imaged in bright-field mode and overlaid with the low-resolution fluorescence image at the correct position (Fig. 5A). The area delimited by the red square is the one selected for the correlation and is represented in all subsequent figures (Figs. 5–7). The number 1 on the rim and the arrow at the centre of the grid were used as landmarks for the correlation in the electron microscope. Then, the fluorescence of the section was imaged at higher resolution. On the ribbon, we detected four consecutive sections. We focused our attention on the first three sections and, more precisely, on two specific cell bodies on each section (Fig. 5B, arrow heads).

After fluorescence imaging, we performed immunogold labelling of GFP with 15 nm size gold particles. The GFP immunogold labelling was chosen to identify the astrocytes in the electron micrograph but also to validate our correlative approach by using the same, labelled protein for light and electron microscopy. It is important to note that after embedding of the labelled section in a thin film of uranyl acetate/methylcellulose, the GFP is quenched (Karreman et al., 2009).

Electron micrographs were recorded using a high-resolution scanning electron microscope with a STEM detector using the Maps software (Fig. 6). Currently this software only operates on

SEM, there for we used a SEM with a STEM detector. This software facilitated the overlay and correlation of light and electron micrographs. Initially, an overview of the grid was taken in the scanning electron microscope in secondary electron mode. Then, the bright-field overview with the low-resolution fluorescence image was imported into Maps and aligned coarsely by matching two pairs of identical points (Fig. 6A; arrows e.g. the central hole of the arrow and a point of number 1 in the grid rim). To improve accuracy of the correlation, a higher resolution STEM (Fig. 6B) image was taken and two conspicuous points visible on the fluorescent image and on the electron micrograph, e.g. border of the cryosection. When needed, this step could be repeated several times at higher magnification. After alignment, the fluorescence image was used to drive the electron microscope stage to the desired areas (arrowheads; Fig. 6C). Afterwards, meshes on the grid containing the ROIs were pre-irradiated (yellow squares; Fig. 6A) with an electron beam to limit contrast differences in the overlapping zone during the acquisition of the tiled images. In the software, a pattern of tiles was laid over the ROI, e.g. 6×6 tiles, and the 3 point focus regime was applied. Usually, focus points were placed top left, middle right and bottom left, just outside the imaging area. Contrast/brightness was kept constant during the acquisition of the tiles. The electron microscope acquired large tile sets of the defined area automatically (e.g. $66 \mu\text{m} \times 57 \mu\text{m} = 3762 \mu\text{m}^2$) down to 3 nm pixel resolution (Fig. 7 and Movie S5). With the HD Viewer, an entire overview could be inspected to get a global picture of the cell interconnections and at the point of interest, one could zoom into the micrograph to observe fine details of the ultrastructure of the sample (Fig. 7, inset).

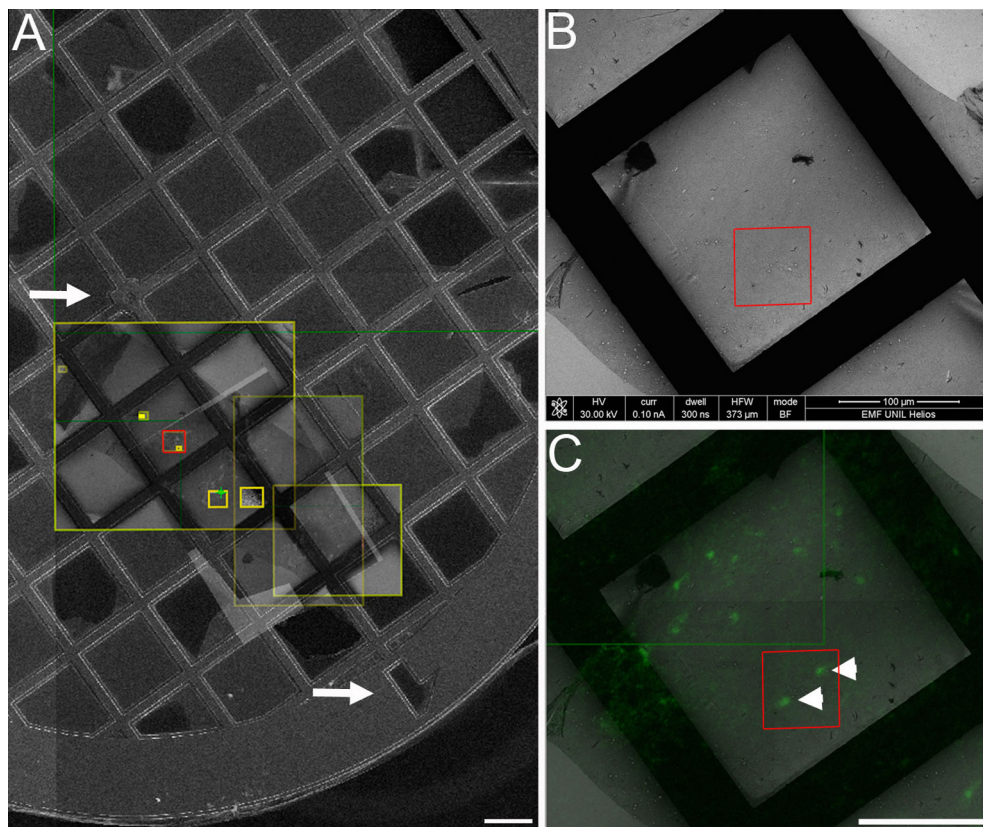


Fig. 6. Correlation of fluorescence image with the electron micrograph. (A) A low-resolution secondary electron micrograph of the grid was recorded with the Maps software. Then, the light micrograph was loaded into the alignment window of the software. In each window, light and electron micrograph, a two-point pointer was placed on the corresponding landmark (arrows). The software uses the pointers to rotate, translate and scale the fluorescence image to exactly match the electron micrograph. (B) STEM image of one section of the ribbon on an EM grid. (C) STEM image overlaid with the fluorescence image. Arrowheads indicate the two cells of interest. The red squares in A, B and C indicate the area imaged at higher resolution and presented in Fig. 7. The yellow squares in A indicate the pre-irradiated areas (Section 2, section STEM imaging). Scale bars represent: A = 200 μm , B = 100 μm , C = 100 μm .

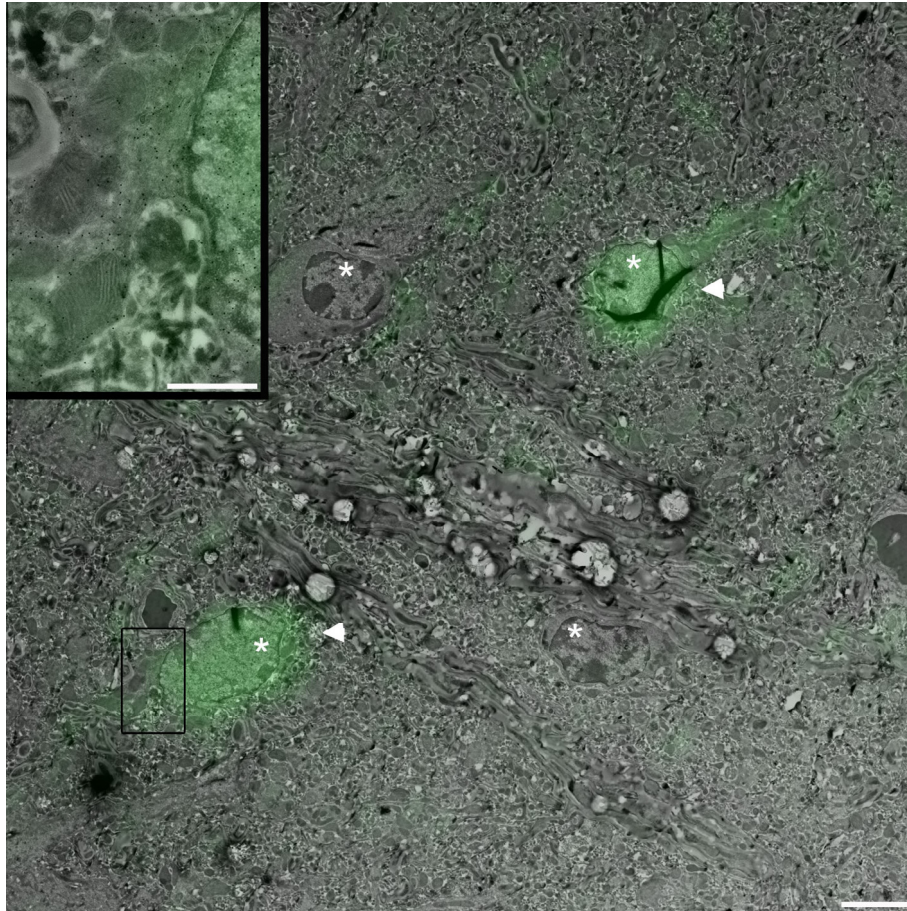


Fig. 7. Large overview of a brain section. With the tiling option of the Maps software, an area of $66 \mu\text{m} \times 57 \mu\text{m}$ was imaged at a pixel resolution of 3 nm. 6×6 tiles were recorded with a frame size of 4096×3536 pixels and a 10% overlap to facilitate stitching. The tiles were stitched in Photoshop. Afterwards, the fluorescence image was overlaid. 4 nuclei (asterisks) can be identified on the micrograph, of which only two matched with the GFP fluorescence (arrowheads). These are the cells indicated with arrowheads in the fluorescence image, Fig. 6C. Zooming into the fluorescent cells, the gold label can be seen (inset). This observation confirms the precise correlation of the fluorescence and gold label signal of the identical protein. The image corresponds to the red squared areas displayed in Figs. 5 and 6. Scale bar represents: $4 \mu\text{m}$. Inset scale bar represents: $1 \mu\text{m}$.

Of the four nuclei visualised on the electron micrograph (asterisks; Fig. 7), two corresponded with the two highlighted spots selected on the fluorescence image (arrowheads, Figs. 6C, 7). By zooming into the electron micrograph on the fluorescent nuclei, the presence of the GFP could be documented by the gold particles (Fig. 7, inset). This observation confirms the accuracy of correlation between the fluorescent signal and the immunogold localised GFP. As GFP is not tagged to the GFA protein but only expressed under the GFAP promoter, the protein is small enough to freely diffuse through the nuclear pores (Seibel et al., 2007). This fact explains the fluorescence and the GFP immunolocalisation of the nucleus of the astrocytes. The accuracy of correlation of the fluorescence image with higher resolution electron micrographs was within $2.11 \mu\text{m}$ before correction. This result was improved by iterative alignment but it was still limited by the resolution of the fluorescence image. Thin astrocyte processes, with a diameter smaller than 20 nm could not be located by fluorescence due to the weak signal emitted but they were easily identified by the immunogold localisation of the GFP (Movie S5; blood vessel surrounded by thin astrocyte process).

Finally, in addition to the resolution of this method, there was good preservation of the astrocyte cytoplasm (Fig. 7 and Movie S5) and of all other cell types (Fig. 2). The cytoplasm has a dense matrix, packed with organelles and vesicles but lacking any striking difference between glial cells or neurons. The notable blemish

of the preparation method was that the large myelinated axons seemed to be poorly embedded in the methylcellulose uranyl acetate film (Fig. 7 and Movie S5).

4. Conclusion

The correlative approach described here allows the localisation of a specific cell subpopulation inside the acute brain slices and their further analysis at nanometre-scale resolution.

An important feature of this approach is that the fluorescence of the GFP label could be preserved throughout the preparation procedure, allowing full control of the area of interest at any time. In fact, with this preparation method, the sample remains in its aqueous environment, which favours the maintenance of GFP fluorescence but is also beneficial to other fluorescent proteins, like ‘tomato’ (unpublished data). In addition, the ultrastructure of the sample prepared according to the Tokuyasu method is well preserved and the strong contrast of the membranes is suitable to investigate vesicles (lysosomes, endosomes, synaptic vesicles) or membrane/membrane interactions. The excellent preservation of the antigenicity of the tissue is also an important factor, and multiple immunolabelling on the same section is possible.

The method was developed for acute brain slices but it is a versatile method that can be applied on various tissue samples. In fact,

we have used it to localise small nerve extensions in mouse skin (unpublished data) and we applied it on yeast cells and plant tissues. It is also important to note that the procedure is fast, and data can be recorded within 3 days.

To conclude, with our combination of fluorescence and electron microscopy following the Tokuyasu protocol, we were able to characterise, at high-resolution, a small biological feature, a “needle”, that was spatially localised and extracted from a significantly larger biological volume, the “haystack”.

Acknowledgments

The authors acknowledge financial support from the Faculty of Biology and Medicine of the University of Lausanne and the Swiss National Science Foundation, R'Equip grant 316030_128692. Advanced ERC grant 340368 “Astromnesia” and Swiss National Science Foundation 31003A 140999 to A. V.”. We thank Dr. G. Knott, CIME, EPFL, for his help with the perfusion fixation experiments, Dr. Matthias Langhorst for fruitful discussions and help with the fluorescence microscopy, Dr. José Maria Mateos for expertise in the neurobiology field and Dr. R. Drillien, IGBMC, for comments on the manuscript.

Appendix A. Supplementary data

Supplementary data associated with this article can be found, in the online version, at <http://dx.doi.org/10.1016/j.jsb.2014.10.011>.

References

- Bethge, P., Chereau, R., Avignone, E., Marsicano, G., Nagerl, U.V., 2013. Two-photon excitation STED microscopy in two colors in acute brain slices. *Biophys. J.* 104, 778–785.
- Collingridge, G.L., 1995. The brain slice preparation: a tribute to the pioneer Henry McIlwain. *J. Neurosci. Methods* 59, 5–9.
- Griffiths, G., 2001. Bringing electron microscopy back into focus for cell biology. *Trends Cell Biol.* 11, 153–154.
- Griffiths, G., Simons, K., Warren, G., Tokuyasu, K.T., 1983. Immunoelectron microscopy using thin, frozen sections: application to studies of the intracellular transport of Semliki forest virus spike glycoproteins. *Methods Enzymol.* 96, 466–485.
- Hayat, M.A., 1981. 3 - Aldehydes. In: Hayat, M.A. (Ed.), *Fixation for Electron Microscopy*. Academic Press, pp. 64–147.
- Huang, B., Babcock, H., Zhuang, X., 2010. Breaking the diffraction barrier: super-resolution imaging of cells. *Cell* 143, 1047–1058.
- Karremans, M.A., Agronskaia, A.V., Verkleij, A.J., Cremers, F.F.M., Gerritsen, H.C., Humbel, B.M., 2009. Discovery of a new RNA-containing nuclear structure in UVC-induced apoptotic cells by integrated laser electron microscopy. *Biol. Cell* 101, 287–299.
- Khurana, S., Li, W.K., 2013. Baptisms of fire or death knells for acute-slice physiology in the age of ‘omics’ and light? *Rev. Neurosci.* 24, 527–536.
- Kirov, S.A., Sorra, K.E., Harris, K.M., 1999. Slices have more synapses than perfusion-fixed hippocampus from both young and mature rats. *J. Neurosci.* 19, 2876–2886.
- Kremer, J.R., Mastronarde, D.N., McIntosh, J.R., 1996. Computer visualization of three-dimensional image data using IMOD. *J. Struct. Biol.* 116, 71–76.
- Kukulski, W., Schorb, M., Welsch, S., Picco, A., Kaksonen, M., Briggs, J.A.G., 2011. Correlated fluorescence and 3D electron microscopy with high sensitivity and spatial precision. *J. Cell Biol.* 192, 111–119.
- Kukulski, W., Schorb, M., Welsch, S., Picco, A., Kaksonen, M., Briggs, J.A.G., 2012. Precise, correlated fluorescence microscopy and electron tomography of Lowicryl sections using fluorescent fiducial markers. In: Thomas, M.-R., Paul, V. (Eds.), *Methods in Cell Biology*. Academic Press, pp. 235–257.
- Liou, W., Geuze, H.J., Slot, J.W., 1996. Improving structural integrity of cryosections for immunogold labeling. *Histochem. Cell Biol.* 106, 41–58.
- Loussert, C., Forestier, C.L., Humbel, B.M., 2012. Correlative light and electron microscopy in parasite research. *Methods Cell Biol.* 111, 59–73.
- Luby-Phelps, K., Ning, G., Fogerty, J., Besharse, J.C., 2003. Visualization of identified GFP-expressing cells by light and electron microscopy. *J. Histochem. Cytochem.* 51, 271–274.
- Mastronarde, D.N., 2005. Automated electron microscope tomography using robust prediction of specimen movements. *J. Struct. Biol.* 152, 36–51.
- McIlwain, H., 1958. Maintenance of the composition of isolated cerebral tissues. *Neurology* 8, 32–33.
- Mironov, A.A., Beznoussenko, G.V., 2009. Correlative microscopy: a potent tool for the study of rare or unique cellular and tissue events. *J. Microsc.* 235, 308–321.
- Modla, S., Czymmek, K.J., 2011. Correlative microscopy: a powerful tool for exploring neurological cells and tissues. *Micron* 42, 773–792.
- Nixon, S.J., Webb, R.L., Floetenmeyer, M., Schieber, N., Lo, H.P., Parton, R.G., 2009. A single method for cryofixation and correlative light, electron microscopy and tomography of zebrafish embryos. *Traffic* 10, 131–136.
- Nolte, C., Matyash, M., Pivneva, T., Schipke, C.G., Ohlemeyer, C., Hanisch, U.K., Kirchhoff, F., Kettenmann, H., 2001. GFAP promoter-controlled EGFP-expressing transgenic mice: a tool to visualize astrocytes and astrogliosis in living brain tissue. *Glia* 33, 72–86.
- Robinson, J.M., Takizawa, T., 2009. Correlative fluorescence and electron microscopy in tissues: immunocytochemistry. *J. Microsc.* 235, 259–272.
- Schwarz, H., Humbel, B.M., 2007. Correlative light and electron microscopy using immunolabeled resin sections. *Methods Mol. Biol. (Clifton, N.J.)* 369, 229–256.
- Seibel, N.M., Eljouni, J., Nalaskowski, M.M., Hampe, W., 2007. Nuclear localization of enhanced green fluorescent protein homomultimers. *Anal. Biochem.* 368, 95–99.
- Slot, J.W., Geuze, H.J., 2007. Cryosectioning and immunolabeling. *Nat. Protoc.* 2, 2480–2491.
- Stephan, A., Mateos, J.M., Kozlov, S.V., Cinelli, P., Kistler, A.D., Hettwer, S., Rulicke, T., Streit, P., Kunz, B., Sonderegger, P., 2008. Neurotrophin cleaves agrin locally at the synapse. *FASEB J.* 22, 1861–1873.
- Stephan, A.H., Madison, D.V., Mateos, J.M., Fraser, D.A., Lovelett, E.A., Coutellier, L., Kim, L., Tsai, H.H., Huang, E.J., Rowitch, D.H., Berns, D.S., Tenner, A.J., Shamloo, M., Barres, B.A., 2013. A dramatic increase of C1q protein in the CNS during normal aging. *J. Neurosci.* 33, 13460–13474.
- Stierhof, Y.D., Schwarz, H., Frank, H., 1986. Transverse sectioning of plastic-embedded immunolabeled cryosections: morphology and permeability to protein A-colloidal gold complexes. *J. Ultrastruct. Mol. Struct. Res.* 97, 187–196.
- Takano, T., He, W., Han, X., Wang, F., Xu, Q., Wang, X., Oberheim Bush, N.A., Cruz, N., Diemel, G.A., Nedergaard, M., 2014. Rapid manifestation of reactive astrogliosis in acute hippocampal brain slices. *Glia* 62, 78–95.
- Takizawa, T., Robinson, J.M., 2003. Correlative microscopy of ultrathin cryosections is a powerful tool for placental research. *Placenta* 24, 557–565.
- Tokuyasu, K.T., 1973. A technique for ultracryotomy of cell suspensions and tissues. *J. Cell Biol.* 57, 551–565.
- Tokuyasu, K.T., 1976. Membranes as observed in frozen sections. *J. Ultrastruct. Res.* 55, 281–287.
- Tokuyasu, K.T., 1978. A study of positive staining of ultrathin frozen sections. *J. Ultrastruct. Res.* 63, 287–307.
- Tsien, R.Y., 1998. The green fluorescent protein. *Annu. Rev. Biochem.* 67, 509–544.
- Zeuschner, D., Geerts, W.J., van Donselaar, E., Humbel, B.M., Slot, J.W., Koster, A.J., Klumperman, J., 2006. Immuno-electron tomography of ER exit sites reveals the existence of free COPII-coated transport carriers. *Nat. Cell Biol.* 8, 377–383.